Available online at www.sciencedirect.com
SCIENCE DIRECT
Microporous and Mesoporous Materials 90 (2006) 307–313
MICROPOROUS AND MESOPOROUS MATERIALS
www.elsevier.com/locate/micromeso

Probing cooperative jump-diffusion in zeolites: Neutron spin–echo measurements and molecular dynamics simulations of benzene in NaX

Hervé Jobic [a,*], Harikrishnan Ramanan [b], Scott M. Auerbach [c,d,*], Michael Tsapatsis [b], Peter Fouquet [e]

[a] Institut de Recherches sur la Catalyse, CNRS, 2 Avenue Albert Einstein, 69626 Villeurbanne, France
[b] Department of Chemical Engineering and Material Science, University of Minnesota, Minneapolis, MN 55455, USA
[c] Department of Chemistry, University of Massachusetts, Amherst, MA 01003, USA
[d] Department of Chemical Engineering, University of Massachusetts, Amherst, MA 01003, USA
[e] Institut Laue Langevin, BP 156, 38042 Grenoble, France

Received 2 September 2005; received in revised form 2 November 2005; accepted 4 November 2005
Available online 22 December 2005

Dedicated to the late Denise Barthomeuf, George Kokotailo and Sergey P. Zhdanov in appreciation of their outstanding contributions to zeolite science

Abstract

We report neutron spin–echo measurements of transport diffusivities for perdeuterated benzene in NaX zeolite. Corrected diffusivities from these neutron measurements were obtained for comparison with recently reported molecular dynamics simulations. Experimental diffusivities were measured with benzene loadings of 1, 2, 3 and 4.5 molecules per NaX cage, and at 300, 350 and 400 K. Both corrected and transport diffusivities increase from 1 to 3 molecules per cage, then decrease sharply to 4.5 molecules per cage. The comparison between experiment and simulation shows remarkably good agreement in both the loading dependence and in the overall magnitudes of the corrected diffusivities, with values mostly in the range 10^{-12}–10^{-11} $m^2 s^{-1}$.

Keywords: Diffusion; Benzene; NaX; Neutron spin–echo; MD simulations

1. Introduction

The transport properties of confined molecules [1,2] play a central role in applications of zeolite–guest systems [3]. A great many experimental and simulation studies have shed light on self-diffusion in zeolites, with a focus on alkanes in siliceous zeolites. These studies have revealed several important phenomena such as single-file self-diffusion [4–6], as well as persistent discrepancies among various microscopic and macroscopic measurements of self-diffusion [7]. Despite these findings, more work is needed before we can use our knowledge of these transport properties to design new processes in zeolites. In particular, more research is needed to understand how the Maxwell–Stefan (also corrected or cooperative) diffusivity, which pertains to non-equilibrium transport, depends on loading and temperature for motion in zeolites [8–11]. In addition, we need greater insights into the transport of unsaturated molecules in non-siliceous zeolites. To address these issues, we report below a combined experimental and simulation study of benzene cooperative diffusion in NaX zeolite.

Among the microscopic methods for measuring diffusion in porous materials, quasi-elastic neutron scattering (QENS) offers the possibility of extracting the self-diffusivity from incoherent neutron scattering, as well as the transport or Fickian diffusivity from coherent neutron scattering

* Corresponding authors.
E-mail addresses: jobic@catalyse.cnrs.fr (H. Jobic), auerbach@chem.umass.edu (S.M. Auerbach).

1387-1811/$ - see front matter © 2005 Elsevier Inc. All rights reserved.
doi:10.1016/j.micromeso.2005.11.006

[12]. Transport diffusivities have been measured by coherent QENS for CF_4 [13], N_2 [14], CO_2 [14] and ethane in silicalite [15], all systems exhibiting relatively facile guest diffusion. The neutron spin–echo (NSE) method provides a way to apply coherent QENS to probe more sluggish motion in zeolites, consisting of rare site-to-site or cage-to-cage jumps. This is crucial for understanding diffusion controlled by shape selectivity. Transport diffusivities of xylenes in BaX [16] and benzene in silicalite [17] have been measured by NSE, which can probe diffusivities two orders of magnitude smaller than those measurable by standard (time-of-flight) QENS. Good agreement between transport diffusivities simulated by molecular dynamics and measured by time-of-flight QENS has been obtained for CF_4 [13], N_2 [14], CO_2 [14], and ethane in silicalite [15]. However, to date no comparison between simulations and NSE transport diffusivities has been reported. Below we pursue this comparison for benzene in NaX, a system with a long history of discrepancies among various probes of diffusion [7].

The direct output from molecular dynamics simulations of cooperative diffusion is the Maxwell–Stefan diffusivity, obtained by correlating collective displacements or velocities [2]. This is related to the transport diffusivity by the equation $D_T = D_{MS} \times \Gamma$, where D_T is the transport diffusivity, D_{MS} the Maxwell–Stefan diffusivity, and Γ is a thermodynamic factor that deviates from unity when the adsorption isotherm exhibits non-ideality [18,19]. Because D_{MS} is a purely dynamical quantity, whereas D_T mixes dynamical and thermodynamic effects, the Maxwell–Stefan diffusivity is often used as the fulcrum for comparing simulations and experiments. For multi-component adsorbed phases, the Maxwell–Stefan diffusivity plays a fundamental role in mixing theories for predicting binary diffusivities from single-component data [20].

Benzene diffusion in NaX is complicated by the interplay of rare site-to-site jumps and strong guest–guest interactions. Kinetic Monte Carlo (KMC) is the method of choice for treating jump diffusion; molecular dynamics is extremely convenient for modeling strong guest–guest interactions; but no simulation method is particularly good at treating both effects. Auerbach and co-workers applied KMC to simulate the loading dependence of benzene self-diffusion in NaX with a rather approximate treatment of guest–guest interactions [21,22]. Though this gave reasonable agreement with the loading dependence of pulsed field gradient (PFG) NMR self-diffusivities [23], we sought in more recent work to relax the assumptions associated with the KMC lattice model. In particular, we applied high temperature molecular dynamics to model both self- and cooperative diffusion of benzene in NaX, yielding excellent agreement for the loading and temperature dependencies of self-diffusion when compared with QENS and PFG NMR data [24]. However, when the simulated Maxwell–Stefan diffusivities were used to compute fluxes for comparison with the membrane permeation data of Nikolakis et al. [25], the simulated fluxes were found to be too high by one or more orders of magnitude [26]. This discrepancy, which may stem from defects in the polycrystalline NaX membranes, calls for a comparison between simulations and a *microscopic* measurement of cooperative benzene diffusion in NaX. Such is provided by the NSE data reported below.

To generate sufficient sampling of cage-to-cage jumps, the molecular dynamics simulations of Ramanan et al. were performed in the temperature range 600–1500 K [24]. In contrast, the NSE data below were obtained at 300–400 K. To compare the two data sets, we extrapolated the simulation results to ambient temperatures as described below. The resulting comparison between experiment and simulation shows remarkably good agreement in both the loading dependence and the absolute Maxwell–Stefan diffusivities, with values mostly in the range 10^{-12}–10^{-11} $m^2 s^{-1}$. This level of agreement augurs well for our growing understanding of cooperative diffusion in complex zeolite–guest systems.

The remainder of this article is organized as follows. In Section 2, we outline the experimental and simulation methods, in Section 3, we give the results, in Section 4, we discuss our findings, and in Section 5, we give a brief summary.

2. Methods

Here we describe the overall system under study, the neutron scattering methodology, and the molecular dynamics simulations.

2.1. System

The FAU framework structure is formed from sodalite cages connected by hexagonal prisms (see Fig. 1). This structure features a large cavity or supercage with four tetrahedrally-located windows (diameter ≈7.5 Å), resulting in a three-dimensional channel system. The unit cell has cubic symmetry and contains eight supercages and eight sodalite cages per unit cell [27]. NaX is a FAU-type zeolite with a Si:Al ratio between 1.0 and 1.5. The material with Si:Al = 1.2 is the most common and thus is studied below; this has 86 Na cations per unit cell compensating the negative charge from the 86 Al atoms in the framework. Benzene readily physisorbs in NaX, binding strongly to Na cations in sites SII, SIII and SIII′ (see Fig. 1). The saturation capacity of benzene in NaX is more than 5 molecules per supercage. Benzene diffusion occurs through jumps among cation sites, leading to cage-to-cage migration and intra-crystalline diffusion.

2.2. NSE measurements

The NaX zeolite (Si:Al = 1.23) previously used for QENS measurements on hydrogenated benzene [28], was activated by heating to 673 K under oxygen flow, and pumped to 10^{-4} Pa at the same temperature. Perdeuterated benzene was adsorbed after cooling. Perdeuterated benzene

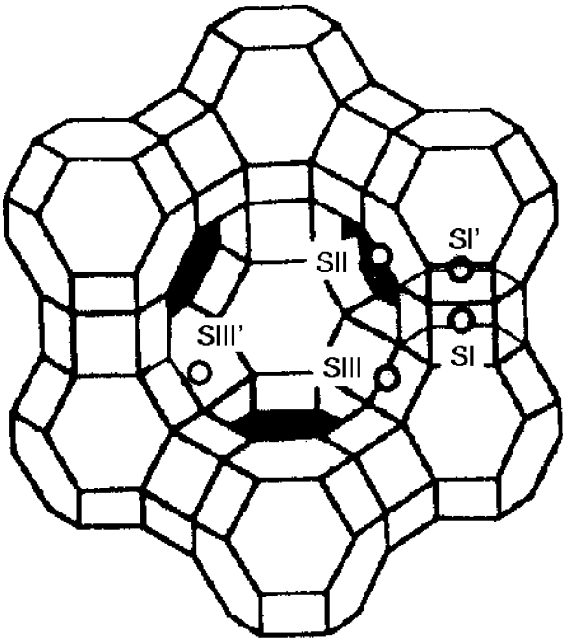

Fig. 1. FAU framework structure showing the cation positions in NaX zeolite. Cation sites SII, SIII and SIII′ interact most strongly with adsorbed benzene.

was used because its coherent neutron scattering cross section is much larger than that of undeuterated benzene [16]. Four samples were prepared with average loadings of 1.0, 2.0, 3.0, and 4.5 molecules per supercage. The samples were transferred into aluminum containers inside a glovebox. The containers were positioned in a furnace, which allowed measurements in the temperature range 300–400 K.

The neutron spin–echo (NSE) experiments were performed at the Institut Laue-Langevin, Grenoble, France, using the IN11 spectrometer [29]. With this spectrometer, the decay of the intermediate scattering function $I(Q,t)$ (the space Fourier transform of the van Hove space–time correlation function) can be traced within a time range of 2 ps to 50 ns. In contrast to time-of-flight spectroscopy, NSE dynamics are obtained directly as a function of time; as such no Fourier transform from energy exchange ω to time t is required. An incident neutron wavelength of 7.4 Å was used throughout. For intensity reasons, wavevector-dependence measurements were restricted to the two Q values 0.2 and 0.3 Å^{-1}, respectively.

Below we report the normalized intermediate scattering function given by

$$\frac{I(Q,t)}{I(Q,0)} = \frac{\int S(Q,\omega)\cos(\omega t)\,\mathrm{d}\omega}{\int S(Q,\omega)\,\mathrm{d}\omega} \tag{1}$$

where $S(Q,\omega)$ is the dynamical structure factor [30]. Due to the high symmetry of benzene, there is no quasi-elastic contribution from rotational motions of the perdeuterated molecule in our Q range. Data for the normalized intermediate scattering function can thus be fitted to the following exponential function corresponding to an isotropic translational motion:

$$\frac{I(Q,t)}{I(Q,0)} = \exp(-D(Q)Q^2 t) \tag{2}$$

where $D(Q)$ is an effective transport diffusivity. One has to sample sufficiently small Q values (corresponding to large distances in real space) to reach the Fickian regime, wherein $D(Q)$ becomes the correct intracrystalline transport diffusivity. Corrected diffusivities were obtained at 300 K by dividing the measured transport diffusivities by appropriate thermodynamic factors [2]. These were calculated from the adsorption data of Doetsch and Ruthven [31], assuming a Langmuir adsorption isotherm with a saturation capacity of 5.5 benzenes per supercage at 300 K [26]. Diffusivities for perdeuterated benzene were converted to those for undeuterated benzene by assuming an inverse-square-root mass dependence, which is standard for pre-exponential factors of diffusion coefficients.

2.3. MD simulations

Simulated corrected (or Maxwell–Stefan) diffusivities were obtained by extrapolating the high-temperature molecular dynamics (MD) results previously reported by Ramanan et al. for benzene in NaX (Si:Al = 1.2) [24]. The details behind these simulations were given in our earlier publication; here we briefly review the salient points. These simulations were performed for temperatures in the range 600–1500 K, and for benzene loadings of infinite dilution, 1, 2, 3 and 4 molecules per cage. For each loading and temperature, several identical runs were performed to assess statistical precision. The guest molecules and Na cations were allowed full motion, while the NaX frame was held fixed for computational efficiency.

The potential function is detailed in Ref. [24]; for completeness we review its construction. The potential energy function takes the form $V = V_{\mathrm{HG}} + V_{\mathrm{G}} + V_{\mathrm{GG}}$, where V_{HG} is the host–guest interaction, V_{G} is the guest internal vibrational potential, and V_{GG} is the guest–guest interaction. The guest vibration term V_{G} is a harmonic valence-bond function fitted to benzene vibrational data [32]. The host–guest term V_{HG} includes electrostatics and Lennard-Jones functions. The zeolite partial charges were fitted to reproduce Na cation distributions in NaX and NaY [33]; while the benzene charges and HG Lennard-Jones parameters were fitted to reproduce the initial heat of adsorption (78 kJ mol^{-1}) and the Na–benzene equilibrium distance (2.7 Å) [24]. The guest–guest term V_{GG} also consists of electrostatics and Lennard-Jones functions. The GG Lennard-Jones parameters were taken from the CVFF forcefield [34].

The cooperative mean square displacement (MSD) was calculated according to [2,8,20]:

$$R^2(t) = \frac{1}{N}\left\langle \left[\sum_{k=1}^{N}\sum_{l=1}^{N}(r_k(\tau+t)-r_k(\tau))\cdot(r_l(\tau+t)-r_l(\tau))\right]\right\rangle \tag{3}$$

where $r_n(\tau)$ is the three-dimensional center-of-mass location of the nth benzene at time τ, and N is the number of benzene molecules in the simulation cell. The long-time slope of the MSD (divided by 6) yields the corrected diffusivity. Slopes were extracted from MSDs in the range 500–3000 Å^2 to ensure that true cage-to-cage motion was sampled (in analogy with sampling small enough Q values in NSE experiments).

The simulations were run at such high temperatures to ensure that sufficient cage-to-cage motion was sampled on a nanosecond time scale. This is crucial for host–guest systems such as benzene in NaX, where aromatic-cation attractions trap guests at sites for long residence times. Sampling methods specialized for rare events, such as transition state theory, have found utility in treating slow self-diffusion in zeolites at infinite dilution, and more recently at finite loadings [35,36]. However, these methods focus on the dynamics of individual molecules perturbed by neighbors, while the NSE measurements probe cooperative motions involving several coupled molecules. We are not aware of a rare-event theory, analogous to transition state theory, that treats cooperative diffusion.

In order to compare with NSE measurements under more ambient conditions, we extrapolated our high-temperature values to lower temperatures assuming an Arrhenius temperature dependence. Such an extrapolation is valid if the basic mechanism for diffusion does not change from high to low temperature. At lower temperatures we surmise that benzene makes rare jumps among supercage Na cations. At higher temperatures, it is possible that cooperative benzene–Na motions may become activated. However, our previous molecular dynamics results show that, even at elevated temperatures, cation motion is localized at sites or within supercages, in contrast to guest motion, which spans many cages [24]. These results lend credence to our overall approach of using high-temperature dynamics to extract low-temperature diffusivities in cation-containing zeolites.

3. Results

Here we report, the results of neutron spin–echo measurements on perdeuterated benzene in NaX, as well as extrapolated molecular dynamics results for benzene in NaX.

3.1. NSE Data

The normalised intermediate scattering functions for perdeuterated benzene in NaX are shown in Fig. 2; they were obtained at $Q = 0.2$ Å^{-1} for a loading of 1 molecule per supercage at temperatures 300, 350 and 400 K. The faster decay of the scattering functions with increasing temperature in Fig. 2 reflects the increase of the diffusivity. Temporal decays extracted from the curves in Fig. 2 were re-expressed as energy broadenings using the time–energy uncertainty relation $\Delta t \Delta E = \hbar$, which gives 1 μs ≈ 1 neV.

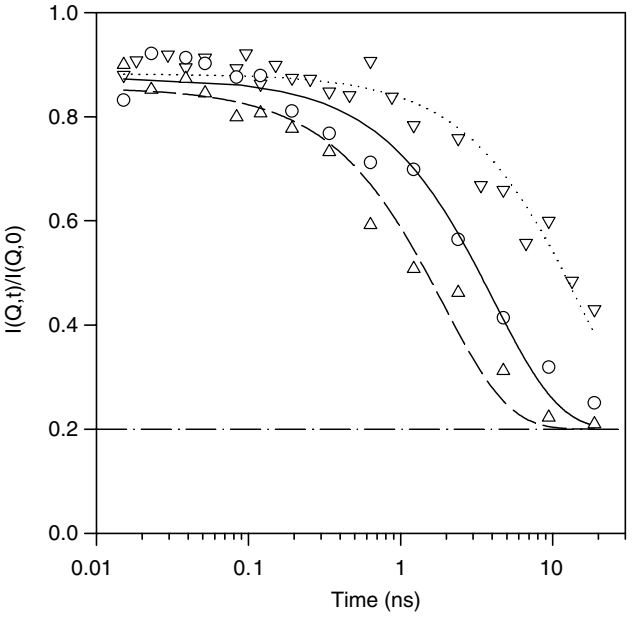

Fig. 2. Normalised intermediate scattering functions obtained for benzene in NaX at: (▽) 300 K, (○) 350 K, and (△) 400 K (loading: 1 molecule per supercage, $Q = 0.2$ Å^{-1}). The dotted-dashed line corresponds to the elastic contribution from the zeolite.

Plotting these energy broadenings against Q^2 should give a linear function if in the Fickian (diffusive) regime. These curves are shown in Fig. 3. A jump-diffusion model [17] was used to fit these data to the solid lines in Fig. 3, from

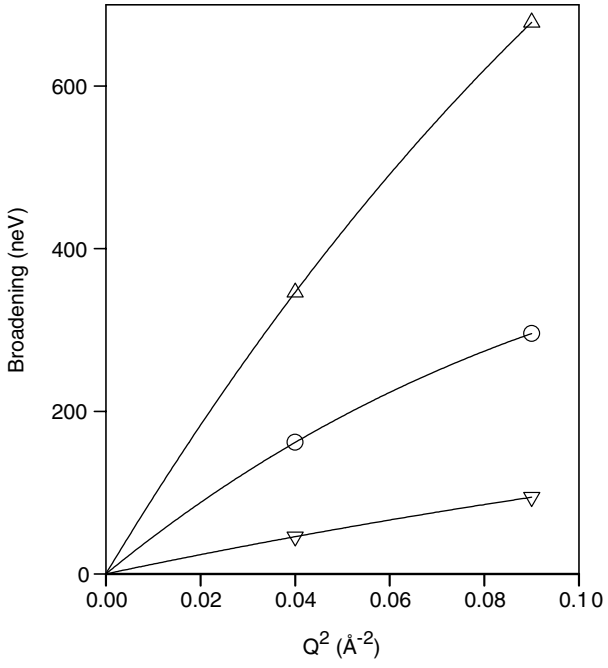

Fig. 3. Broadenings obtained for benzene in NaX at: (▽) 300 K, (○) 350 K, and (△) 400 K (loading: 1 molecule per supercage). The points are obtained from the normalised intermediate scattering functions measured at $Q = 0.2$ and 0.3 Å^{-1}; the solid lines correspond to a jump diffusion model.

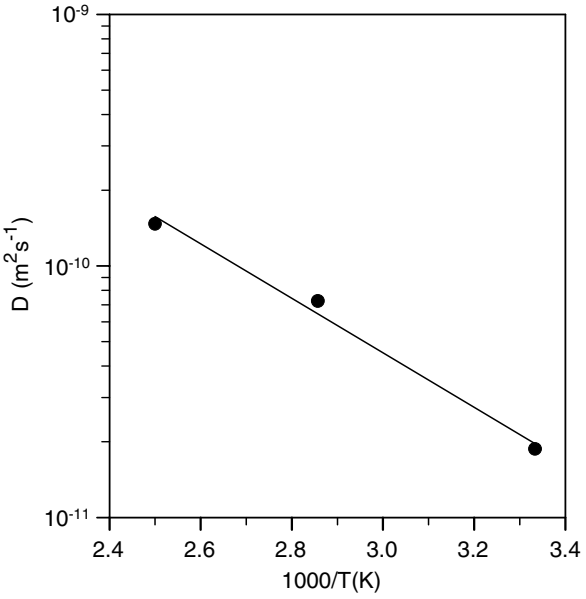

Fig. 4. Arrhenius plot of the transport diffusivities of benzene in NaX, obtained for a loading of 1 molecule per supercage.

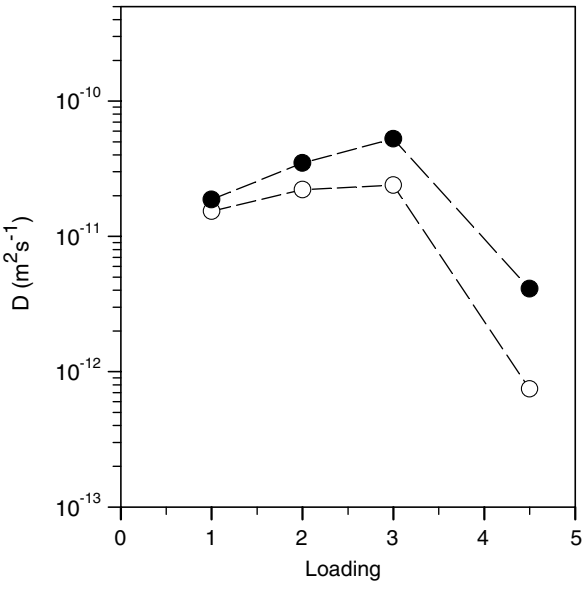

Fig. 6. Diffusivities determined by NSE at 300 K for perdeuterated benzene in NaX zeolite: (●) transport diffusivities, (○) corrected diffusivities.

which diffusivities were extracted from the low-Q slopes. Transport diffusivities for a loading of 1 molecule per cage are shown in Fig. 4 as a function of temperature. The apparent activation energy at this loading is 20.7 kJ mol^{-1}.

The normalised intermediate scattering functions measured at 300 K for loadings of 1.0, 2.0 and 3.0 molecules per cage are shown in Fig. 5. The faster decay observed for increasing benzene loading indicates that the transport diffusivity steadily increases with loading in this regime, in contrast to the results for self-diffusion. The transport diffusivities obtained at 300 K are shown in Fig. 6 as a function of perdeuterated benzene loading. Corrected diffusivities for perdeuterated benzene are also shown in Fig. 6 as a function of loading. These were obtained from the transport diffusivities in Fig. 6 by dividing by the appropriate thermodynamic correction factors. Finally, the corrected diffusivities for undeuterated benzene in NaX at 300 K, after mass scaling, are shown as a function of loading in Fig. 7. Experimental error bars are indicated.

3.2. Simulation data

Fig. 7 shows the extrapolated corrected diffusivity as a function of loading at 300 K. The MD simulations

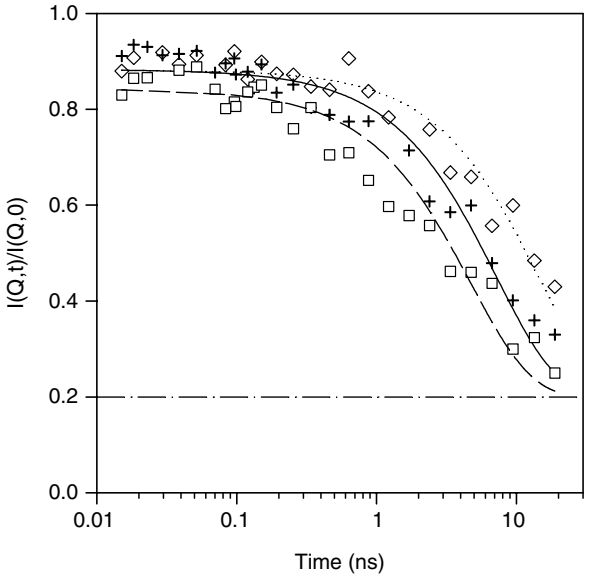

Fig. 5. Normalised intermediate scattering functions obtained for benzene in NaX at 300 K, at different loadings: (◇) 1, (+) 2, and (□) 3 molecules per supercage ($Q = 0.2$ Å^{-1}).

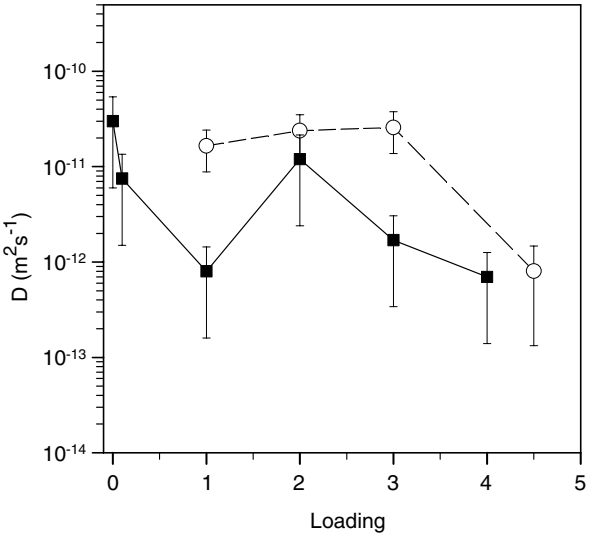

Fig. 7. Comparison of corrected diffusivities for benzene in NaX at 300 K: (○) NSE, (■) MD simulations.

performed by Ramanan et al. [24] cover the range of loadings from infinite dilution to four benzenes per supercage. The error bars for the extrapolated corrected diffusivities in Fig. 7 are estimated from errors propagated to the apparent activation energies extracted from high-temperature MD results [24].

4. Discussion

The temperature dependence of diffusion typically follows an Arrhenius behavior with the apparent activation energy corresponding to an effective barrier for cage-to-cage motion. The self- and corrected diffusivities can in general exhibit different apparent activation energies. The apparent activation energy for benzene self-diffusion in NaX falls in the range of 20–25 kJ mol^{-1} [28]. The NSE results above find a value of 20.7 kJ mol^{-1} for corrected diffusion, indicating that self- and corrected diffusion of benzene in NaX experience very similar cage-to-cage barriers.

The loading dependence of diffusion typically shows a decreasing trend at high loadings as blocking of diffusion pathways slows transport. At low to intermediate loadings, both increasing and decreasing trends are possible for the self- [22] and corrected diffusivities [38]. Kinetic Monte Carlo [22] and molecular dynamics simulations [24] agree with QENS [37] and PFG NMR experiments [23] that the self-diffusivity for benzene in NaX follows a monotonically decreasing trend. The corrected and transport diffusivities measured by NSE show a mild increasing trend from 1.0 to 3.0 molecules per cage, followed by a sharp decrease at 4.5 molecules per cage. In spite of experimental error, Fig. 5 shows that the increasing trend at low to intermediate loadings appears to be statistically significant. This loading dependence is then qualitatively different from that found for self-diffusion of benzene in NaX.

The corrected diffusivities of CF_4 [13], CO_2 [14], and ethane in silicalite [15] all show a monotonically decreasing loading dependence, as determined by coherent QENS and cooperative MD simulations. In contrast, the corrected diffusivity of N_2 in silicalite shows a very weak maximum [14]. The mechanisms underlying the loading dependencies for benzene in NaX and N_2 in silicalite are likely very different. In the former case, benzene molecules attract one another strongly from specific adsorption sites; whereas in the latter case, N_2 molecules diffuse on a relatively flat energy landscape and feel negligible sorbate–sorbate interactions. It is thus not obvious why these systems should behave similarly viz. their corrected diffusivities. To address such issues, Krishna and co-workers have reported KMC studies that reveal how various topologies and sorbate–sorbate interactions influence the loading dependence of corrected (Maxwell–Stefan) diffusion [9–11]. These studies aim to connect with the analytical mean-field results reported by Reed and Ehrlich for a lattice of identical adsorption sites [38]. To shed light on benzene cooperative diffusion in NaX, which samples a collection of heterogeneous sites, more theoretical research is needed to reveal how such heterogeneous host–guest interactions influence the loading dependence of cooperative diffusion [39].

The comparison between the corrected diffusivities of benzene in NaX obtained from NSE experiments and MD simulations is shown in Fig. 7. The comparison between experiment and simulation shows remarkably good agreement in both the loading dependence and in the overall magnitudes of the corrected diffusivities, with values mostly in the range 10^{-12}–10^{-11} m^2 s^{-1}. The biggest discrepancy in magnitude arises for a loading of 1 molecule per cage, where simulations predict an order-of-magnitude decrease in diffusivity compared to adjacent loadings. Such a strong loading dependence would seem anomalous, and may stem from propagated error in the extrapolation from high temperatures. Indeed, the experimental activation energy for 1 molecule per cage is 20.7 kJ mol^{-1}, while that from simulation is 36.4 kJ mol^{-1}, consistent with a low MD diffusivity. On the other hand, simulated activation energies for infinite dilution and 2 molecules per cage are 27.4 and 24.7 kJ mol^{-1}, respectively, both in reasonable agreement with experiment. More extensive simulations may be required to resolve the issue for 1 molecule per cage, possibly providing more statistically reliable diffusivity data at this loading. Despite this fact, the otherwise broad agreement between experiment and simulation is quite encouraging.

5. Summary

We have reported a combined neutron scattering and molecular dynamics (MD) simulation study of cooperative benzene diffusion in NaX zeolite. Experimental transport diffusivities were obtained by performing neutron spin–echo (NSE) measurements on perdeuterated benzene in NaX. Corrected diffusivities were then obtained by dividing the transport diffusivities by the appropriate thermodynamic factors. Simulated corrected diffusivities were obtained by extrapolating high-temperature MD results to lower temperatures. Experimental diffusivities were measured with benzene loadings of 1, 2, 3 and 4.5 molecules per NaX cage, and at 300, 350 and 400 K. Both corrected and transport diffusivities increase from 1 to 3 molecules per cage, then decrease sharply to 4.5 molecules per cage. The comparison between experiment and simulation shows remarkably good agreement in both the loading dependence and in the overall magnitudes of the corrected diffusivities, with values mostly in the range 10^{-12}–10^{-11} m^2 s^{-1}. This broad agreement lends credence to the use of NSE measurements for probing cooperative diffusion in zeolites. Such measurements could complement existing characterization methods, possibly shedding light on grain boundaries and other defects that impact transport in zeolites [40].

Acknowledgement

H.R., M.T. and S.M.A. acknowledge generous support from Raul Miranda at the Department of Energy under

Grant number DE-FG02-94ER14485, the National Science Foundation (NSF CTS-0091406) and the National Environmental Technology Institute (NETI), for supporting research on diffusion in zeolites. H.J. thanks the Institut Laue-Langevin, Grenoble, France, for the allocated beam time.

References

[1] J. Karger, D.M. Ruthven, Diffusion in Zeolites and Other Microporous Solids, John Wiley & Sons, New York, 1992.
[2] J. Karger, S. Vasenkov, S.M. Auerbach, in: S.M. Auerbach, K.A. Carrado, P.K. Dutta (Eds.), Handbook of Zeolite Science and Technology, Marcel-Dekker, New York, 2003, p. 341.
[3] S.M. Auerbach, K.A. Carrado, P.K. Dutta (Eds.), Handbook of Zeolite Science and Technology, Marcel Dekker, Inc., New York, 2003.
[4] V. Gupta, S.S. Nivarthi, A.V. McCormick, H.T. Davis, Chem. Phys. Lett. 247 (1995) 596.
[5] K. Hahn, J. Karger, V. Kukla, Phys. Rev. Lett. 76 (1996) 2762.
[6] H. Jobic, K. Hahn, J. Karger, M. Bee, A. Tuel, M. Noack, I. Girnus, G.J. Kearley, J. Phys. Chem. B 101 (1997) 5834.
[7] S. Brandani, Z. Xu, D. Ruthven, Micropor. Mater. 7 (1996) 323.
[8] M.J. Sanborn, R.Q. Snurr, AICHE J. 47 (2001) 2032.
[9] R. Krishna, D. Paschek, R. Baur, Micropor. Mesopor. Mater. 76 (2004) 233.
[10] R. Krishna, J.M. van Baten, D. Dubbeldam, J. Phys. Chem. B 108 (2004) 14820.
[11] R. Krishna, J.M. van Baten, Chem. Eng. Technol. 28 (2005) 160.
[12] H. Jobic, J. Karger, M. Bee, Phys. Rev. Lett. 82 (1999) 4260.
[13] H. Jobic, A.I. Skoulidas, D.S. Sholl, J. Phys. Chem. B 108 (2004) 10613.
[14] G.K. Papadopoulos, H. Jobic, D.N. Theodorou, J. Phys. Chem. B 108 (2004) 12748.
[15] S.-S. Chong, H. Jobic, M. Plazanet, D.S. Sholl, Chem. Phys. Lett. 408 (2005) 157.
[16] H. Jobic, A. Methivier, G. Ehlers, Micropor. Mesopor. Mater. 56 (2002) 27.
[17] H. Jobic, M. Bée, S. Pouget, J. Phys. Chem. B 104 (2000) 7130.
[18] R. Krishna, Chem. Eng. Sci. 48 (1993) 845.
[19] R. Krishna, J.A. Wesselingh, Chem. Eng. Sci. 52 (1997) 861.
[20] A.I. Skoulidas, D.S. Sholl, R. Krishna, Langmuir 19 (2003) 7977.
[21] C. Saravanan, F. Jousse, S.M. Auerbach, Phys. Rev. Lett. 80 (1998) 5754.
[22] C. Saravanan, S.M. Auerbach, J. Chem. Phys. 110 (1999) 11000.
[23] A. Germanus, J. Karger, H. Pfeifer, N.N. Samulevic, S.P. Zdanov, Zeolites 5 (1985) 91.
[24] H. Ramanan, S.M. Auerbach, M. Tsapatsis, J. Phys. Chem. B 108 (2004) 17171.
[25] V. Nikolakis, G. Xomeritakis, A. Abibi, M. Dickson, M. Tsapatsis, D.G. Vlachos, J. Membr. Sci. 184 (2001) 209.
[26] H. Ramanan, S.M. Auerbach, M. Tsapatsis, J. Phys. Chem. B 108 (2004) 17179.
[27] W.M. Meier, D.H. Olson, C. Baerlocher, Atlas of Zeolite Framework Types, Elsevier, Amsterdam, New York, 2001.
[28] H. Jobic, A.N. Fitch, J. Combet, J. Phys. Chem. B 104 (2000) 8491.
[29] B. Farago, Physica B 268 (1999) 270.
[30] L. van Hove, Phys. Rev. 95 (1954) 249.
[31] D.M. Ruthven, I.H. Doetsch, AICHE J. 22 (1976) 882.
[32] S.M. Auerbach, N.J. Henson, A.K. Cheetham, H.I. Metiu, J. Phys. Chem. 99 (1995) 10600.
[33] E. Jaramillo, S.M. Auerbach, J. Phys. Chem. B 103 (1999) 9589.
[34] C. Blanco, S.M. Auerbach, J. Phys. Chem. B 107 (2003) 2490.
[35] C. Tunca, D.M. Ford, J. Chem. Phys. 111 (1999) 2751.
[36] E. Beerdsen, B. Smit, D. Dubbeldan, Phys. Rev. Lett. 93 (2004) 248301.
[37] H. Jobic, M. Bee, J. Karger, H. Pfeifer, J. Caro, J. Chem. Soc.-Chem. Commun. (1990) 341.
[38] D.A. Reed, G. Ehrlich, Surf. Sci. 102 (1981) 588.
[39] A.I. Skoulidas, D.S. Sholl, J. Phys. Chem. B 109 (2005) 15760.
[40] S. Vasenkov, W. Bohlmann, P. Galvosas, O. Geier, H. Liu, J. Karger, J. Phys. Chem. B 105 (2001) 5922.